



HAL
open science

MicroVIP: Microscopy image simulation on the Virtual Imaging Platform

Ahmad Ali, Guillaume Vanel, Sorina Camarasu-Pop, Axel Bonnet, Carole Frindel, David Rousseau

► **To cite this version:**

Ahmad Ali, Guillaume Vanel, Sorina Camarasu-Pop, Axel Bonnet, Carole Frindel, et al.. MicroVIP: Microscopy image simulation on the Virtual Imaging Platform. *SoftwareX*, 2021, 16, pp.100854. 10.1016/j.softx.2021.100854 . hal-03619436

HAL Id: hal-03619436

<https://hal.science/hal-03619436v1>

Submitted on 5 Jan 2024

HAL is a multi-disciplinary open access archive for the deposit and dissemination of scientific research documents, whether they are published or not. The documents may come from teaching and research institutions in France or abroad, or from public or private research centers.

L'archive ouverte pluridisciplinaire **HAL**, est destinée au dépôt et à la diffusion de documents scientifiques de niveau recherche, publiés ou non, émanant des établissements d'enseignement et de recherche français ou étrangers, des laboratoires publics ou privés.



Distributed under a Creative Commons Attribution - NonCommercial 4.0 International License

MicroVIP: Microscopy image simulation on the Virtual Imaging Platform

Ali Ahmad^{a,b}, Guillaume Vanel^a, Sorina Camarasu-Pop^a, Axel Bonnet^a,
Carole Frindel^a, David Rousseau^{b,*}

^a*Centre de Recherche en Acquisition et Traitement de l'Image pour la Santé (CREATIS),
CNRS UMR 5220 – INSERM U1206, Université Lyon 1, Insa de Lyon, Lyon, France*

^b*Laboratoire Angevin de Recherche en Ingénierie des Systèmes (LARIS), UMR INRAE
IRHS, Université d'Angers, 62 Avenue Notre Dame du Lac, 49000 Angers, France*

Abstract

MicroVIP is an open source software that assembles, in a unified web-application running on distributed computing resources, simulators of the main fluorescent microscopy imaging modalities (with existing codes or newly developed). MicroVIP provides realistic simulated images including several sources of noise (microfluidic blur effect, diffraction, Poisson noise, camera read out noise). MicroVIP also includes a module which simulates single cells with fluorescent markers and a module to analyse the simulated images with textural and pointillist feature spaces. MicroVIP is shown to be of value for supervised machine learning. It allow to automatically generate large sets of training images and virtual instrumentation to optimize the optical parameters before realizing real experiments.

Keywords: Microscopy image simulation, Virtual Imaging Platform, Machine learning

*Corresponding author: D. ROUSSEAU (e-mail: david.rousseau@univ-angers.fr).

Code Metadata

Nr.	Code metadata description	Please fill in this column
C1	Current code version	1.0.1
C2	Permanent link to code/repository used for this code version	https://gitlab.in2p3.fr/guillaume.vanel/microvip/-/tree/1.0.1
C3	Code Ocean compute capsule	None
C4	Legal Code License	GNU GPL
C5	Code versioning system used	git
C6	Software code languages, tools, and services used	MATLAB
C7	Compilation requirements, operating environments & dependencies	MATLAB Compiler and Runtime, Linux
C8	If available Link to developer documentation/manual	https://gitlab.in2p3.fr/guillaume.vanel/microvip/-/wikis/home
C9	Support email for questions	guillaume.vanel@creatis.insa-lyon.fr

Table 1: Code metadata

1. Motivation and significance

Microscopy has benefited from several revolutions in the last two decades. It is now possible to perform 3D imaging, super-resolution or highlight targeted molecules with fluorescent markers. The power of these modern microscopes is further enhanced when they are coupled to microfluidic systems automatically conveying the samples under the microscope, or when images are fed to machine learning algorithms to automate image processing. In this context, a large number of imaging systems are available for a given bioimaging question. On the instrumentation side, comparing all methods on the same sample can be time consuming. On the computational side, in era of machine learning-based image processing, the design of algorithms is driven by the need of annotated data which are also time consuming to produce. One way to overcome these bottlenecks in the optimization of instrumentation or the design of supervised machine learning algorithms is to use simulation.

Many fluorescence microscopy simulators have been proposed in the literature: for example the widefield image simulators SIMCEP and PSFGenerators [1, 2, 3], the confocal image simulators ConfocalGN, CytoPacq, and PSFLab [4, 5, 6], the super-resolution simulation tools SOFI, SuReSIM and

20 FluoSim [7, 8, 9] or the LSM simulation tool Biobeam [10], etc. However,
 21 these tools are usually specific to a single microscopy technique. They also
 22 lack standardization, and thus do not share common sets of inputs or outputs,
 23 no common programming languages, nor common interface.

24 We present an open source software which assembled most fluorescent
 25 microscopy simulators in a unified web-application that runs on a large dis-
 26 tributed computing infrastructure.

27 We demonstrate its value both for virtual instrumentation and for boost-
 28 ing data annotation in supervised machine learning problems.

29 2. Software description

30 In this section, we present the architecture, functionalities and illustra-
 31 tive examples of the MicroVIP software. For more details about the code,
 32 inputs and outputs, please refer to each module page at the project’s wiki
 33 documentation: <https://gitlab.in2p3.fr/guillaume.vanel/microvip/-/wikis/home>.
 34

35 2.1. Software Architecture

36 MicroVIP offers a complete simulation pipeline in three main steps de-
 37 scribed below and represented in Figure 1.

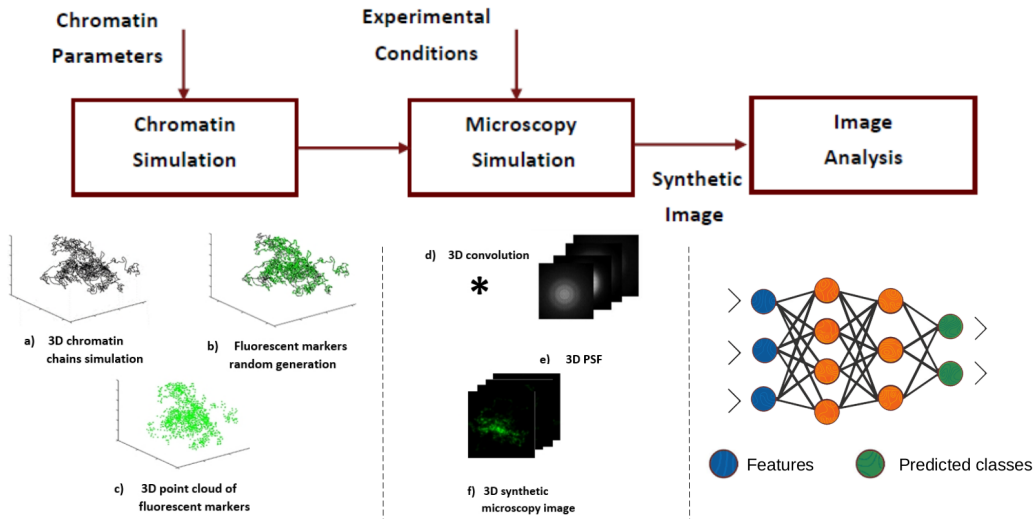


Figure 1: Global architecture of MicroVIP. It consists in three concatenated main modules assembled in a pipeline. The first one generates synthetic biological objects. The second module stands for the simulation of microscopy images of the synthetic biological object. The third module extracts characteristics of the simulated images.

38 *2.1.1. Module 1: Generation of biological objects*

39 Module 2 can load any type of 3D fluorescent point cloud. To offer a
40 baseline we created Module 1 which models chromatin (mimicking the yeast
41 genome as described in [11]) in a single cell. For each chromatin chain,
42 100 configurations have been modeled beforehand using InfMod3DGen [11].
43 MicroVIP generates fluorescent markers placed along these chains, with dis-
44 tances between two consecutive markers drawn from a random distribution
45 parameterized by the user (see 2.2.2). This module outputs the list of 3D
46 markers coordinates (see 2.2.3), used as input of module 2.

47 *2.1.2. Module 2: Microscopy image simulation*

48 In this module, the synthetic microscopy images are generated from the
49 3D fluorescent markers point cloud produced by previous module or di-
50 rectly loaded by the user. Various fluorescence microscopy techniques can
51 be simulated, such as wide field microscopy (WFM), confocal microscopy
52 (CFM) [12], structured illumination microscopy (SIM) [13], light sheet mi-
53 croscopy (LSFM) [14, 15], and super resolution microscopy (SMLM) [16].
54 All simulation codes are, so far, original except for the SIM [17, 18]. More-
55 over, this module enables imaging simulation for moving samples as found
56 in microfluidic systems. Image acquisition is simulated taking into account
57 biomarkers photobleaching, light diffraction within the optical system, signal
58 noises at the camera sensor and motion blur in the case of microfluidics in
59 order to produce an as realistic output 3D synthetic microscopy image as
60 possible. As detailed in 2.2.2, the complete optical and image acquisition
61 system is adjustable. An illustration of simulated images produced with this
62 module is given in Figure 2. MicroVIP includes just the production of im-
63 ages (in .tiff format) which can then be exported and visualized with any
64 standard visualizing tool.

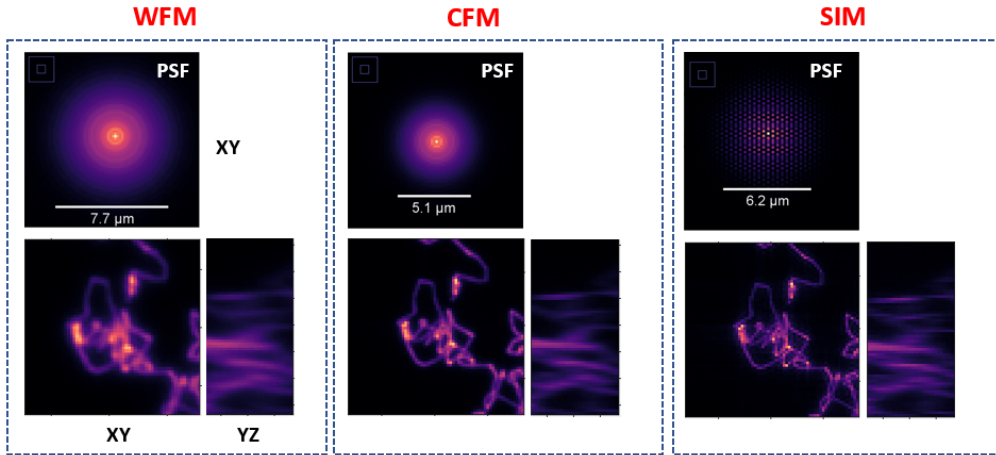


Figure 2: Images simulated using MicroVIP module 2 with various microscopy techniques. WFM: widefield microscopy , CFM: confocal microscopy and SIM: structured illumination microscopy. Only two chromatin chains are shown for better visualization. Optical parameters are: 40x objective lens, water medium (refractive index 1.33), numerical aperture 0.95 and laser emission wavelength 561nm.

65 *2.1.3. Module 3: Features extraction*

66 This is the module responsible for the application of several features ex-
 67 traction methods on the synthetic 3D image obtained at previous module.
 68 Three types of features are extracted, as described in [19, 20]: 2D textural
 69 features computed from the sum z-projection of the 3D microscopy image,
 70 3D textural features extracted directly from the 3D image, and pointillist
 71 features. These latter describe the distribution of biomarker positions. They
 72 require a beforehand particle localization and are applied not to the image
 73 directly but to the localized 3D marker coordinates.

74 Textural features include the auto-correlation function for 2D images, lo-
 75 cal binary patterns (LBP) [21, 22], gray-level coocurrence matrix (GLCM) [23,
 76 24] and scattering transform (scatnet) [25] for 2D and 3D images. Pointillist
 77 features consist in characteristics computed from K-Ripley’s function [26, 19].
 78 The particle localization is performed using third-party tool UNLOC de-
 79 tect [27] which has been integrated to this module.

80 All methods’ hyper-parameters can be adjusted as described in 2.2.2, and
 81 for each of them a 1D numerical features vector is obtained, ready to use for
 82 machine learning algorithms.

83 *2.2. Software Functionalities*

84 *2.2.1. Interface*

85 MicroVIP's interface is reproduced in Figure 3. It requires only five user
86 inputs described below.

87 *Execution name.* This field enables users to provide a name identifying their
88 execution in order to monitor its progress in VIP. One can notably see the
89 inputs and outputs used for an execution, and access execution logs as well
90 as data and charts to visualize file transfer and computation times.

91 *Results directory.* This is a logical path inside VIP File Transfer structure
92 where execution outputs will be made accessible.

93 *Number of cells.* This is the number of statistically independent instances
94 MicroVIP has to run with the same set of parameters except for the seed
95 (which must be different). This allows generation of simulated data for a
96 whole population of cells modeled with the same biological parameters and
97 imaged with the same microscopy setup. MicroVIP instances are launched in
98 parallel on European Grid Infrastructure (EGI), enabling a significant time
99 gain in data generation compared to multiple successive MicroVIP executions
100 (see 5.1).

101 *Pipeline.* We introduced this input for flexibility of MicroVIP pipeline with
102 regards to the user's needs. It takes values 0, 1 and 2 and allows one to
103 execute only the first module, the first two modules, or all three of them re-
104 spectively. In other words, it dictates if simulation should stop after ground
105 truth modeling (0), continue until microscopy image simulation (1) or also
106 perform features extraction (2). It mostly exists to avoid the time consum-
107 ing extraction of multiple features when the user only needs the simulated
108 images.

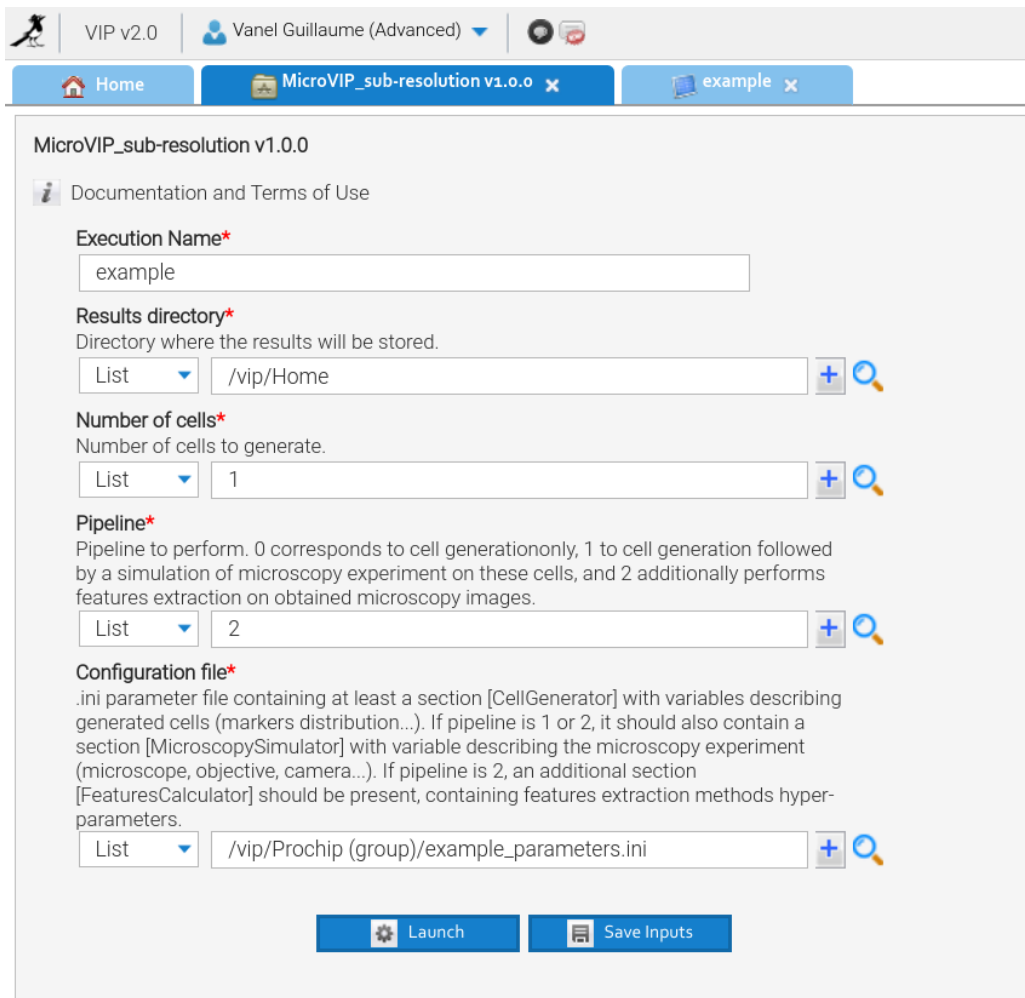


Figure 3: MicroVIP graphical user interface, available in VIP after creating a free account and joining the open access group Prochip, at <https://vip.creatis.insa-lyon.fr>

109 *2.2.2. Configuration file*

110 The last user input is a .ini text file containing all necessary parameters
 111 for each of the three MicroVIP modules. It gives MicroVIP the ability to be
 112 completely adaptable and customizable while maintaining the accessibility
 113 offered by a trivial graphical user interface. Several example files are avail-
 114 able on VIP, and one of them is given in Appendix A. .ini is a standard
 115 file format for configuration files. It allows definition of parameter values as
 116 well as comments, and can be structured in several sections. MicroVIP con-
 117 figuration file takes advantage of these features, providing a comprehensive
 118 description of each parameter, and grouping them in sections corresponding

119 to the module they play a role in.

120 2.2.3. Output

121 After completion of a MicroVIP execution, the user can find and download
122 a .tar archive at the location they chose inside VIP File Transfer architecture.
123 This archive is structured in four sub-directories, some of which may be
124 empty if input parameter *pipeline* has been set to less than 2 (see 2.2.1).

125 *markers_coordinates*. This directory contains modelled ground truth biomarker
126 3D point clouds, stored as three columns .csv file representing each marker
127 3-D coordinates (x, y, z) in μm , centered around 0. This will never be an
128 empty directory.

129 *ground_truth_images*. This folder contains ground truth 3D image stacks of
130 the biomarkers. These are binary images with value one where markers are
131 present and zero everywhere else. They have the same size as final simulated
132 microscopy images, and are stored in .tif file format. This directory will be
133 empty if module 2 is not executed (*pipeline* value 0).

134 *final_images*. This directory contains simulated microscopy 3D image stacks
135 in .tif file format. It will be empty if module 2 is not executed (*pipeline* value
136 0).

137 *extracted_features*. This folder contains 2D, 3D and pointillist features ex-
138 tracted for each simulated image. These are stored in .json file format, in
139 a JSON object with keys "2D", "3D" and "Pointillist". Each key refers
140 to a JSON object mapping features extraction method names to 1D fea-
141 tures vectors. More information can be found at [https://gitlab.in2p3.
142 fr/guillaume.vanel/microvip/-/wikis/Features](https://gitlab.in2p3.fr/guillaume.vanel/microvip/-/wikis/Features). This directory will be
143 empty if MicroVIP module 3 is not executed (*pipeline* value 0 or 1).

144 To provide an example, a simulation run with *Number of cells* 2, *pipeline*
145 2 and *Configuration file* widefield.ini will result in following output architec-
146 ture:

```
microVipOut.tar
├── markers_coordinates
│   ├── 1of2_widefield.ini.csv
│   └── 2of2_widefield.ini.csv
├── ground_truth_images
│   ├── 1of2_widefield.ini.gt.tif
│   └── 2of2_widefield.ini.gt.tif
└── final_images
```

```
├── 1of2_widefield.ini.img.tif
├── 2of2_widefield.ini.img.tif
├── extracted_features
├── 1of2_widefield.ini.json
└── 2of2_widefield.ini.json
```

147 3. Application

148 MicroVIP can be used for a variety of microscopy applications. In partic-
149 ular, it can be used for research and development in bioimaging application
150 such as single cell imaging (which is natively included in the platform). Ad-
151 ditionally, it can be used for virtual instrumentation by realising low cost and
152 fast in silico tests to determine the best tools and settings before a real mi-
153 croscopy experiment. Moreover, MicroVIP can be used for machine learning
154 applications such as deep learning based super-resolution, also style transfer
155 from an imaging modality to another, or data augmentation as it enables
156 fast and inexpensive realization of a 3D microscopy images database with as-
157 sociated ground truth, for calibration and training of image analysis and/or
158 cell image classification tools. Moreover, the software allows to answer these
159 problems in a centralized way for a variety of microscopy techniques.

160 4. Illustrative Example

161 MicroVIP already enabled to discover non intuitive regimes where sub-
162 resolved low-cost microscopes could perform as well as expansive super-
163 resolved microscopes for cell sorting [19, 20]. We provide another example
164 where MicroVIP simulator is used to generate synthetic 3D light-sheet flu-
165 orescence microscopy images acquired in a microfluidic system with a flow
166 rate of 50 *nl/min* with objective lens=60x, water immersion and NA=1.1.
167 Generated images and their ground truth were used to train the deep learn-
168 ing Content Aware Image Restoration (CARE) denoising model [28]. The
169 model trained on synthetic data was then used to denoise real microscopy
170 images acquired in the same conditions.

171 Images were simulated by adapting MicroVIP configuration file (see 2.2.2)
172 to match the real acquisition parameters. Figure 4 shows an illustration of
173 simulated image and its associated ground truth binary image, as well as the
174 result of denoising a real image.

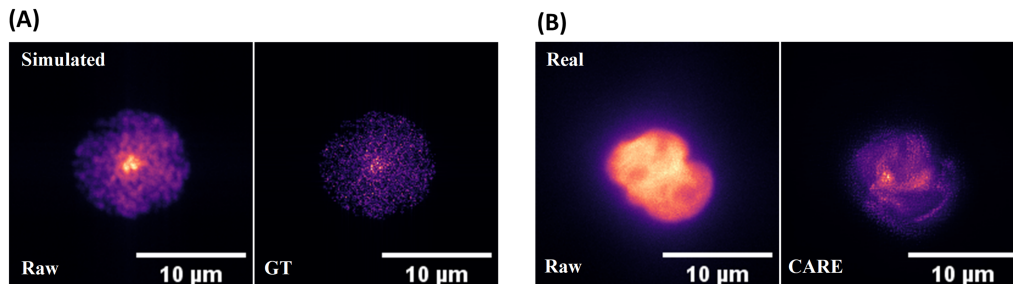


Figure 4: Illustrative example of MicroVIP application for data augmentation. **(A)** maximum z-projection planes of simulated 3D light-sheet fluorescence microscopy image and its associated ground truth. **(B)** results of real light sheet microscopy image denoising using CARE model pre-trained with synthetic images generated with MicroVIP.

175 5. Impact

176 MicroVIP possibly interests several scientific communities including: (i)
 177 computer scientists interested in data challenge on bioimaging since they
 178 need large amount of annotated data sets, (ii) physicists interested in opti-
 179 mizing optical parameters with virtual instrumentation and (iii) biologists
 180 specialized in chromatin imaging in single cell (since this use case is already
 181 fully implemented). The impact of MicroVIP will be enhanced, as described
 182 in this section, thanks to the deployment of MicroVIP on the resources of
 183 the EGI e-infrastructure and via the availability of tutorials.

184 5.1. Virtual Imaging Platform

185 MicroVIP is deployed on the virtual imaging platform (VIP) [29]. VIP
 186 is a web portal for simulation and analysis of medical images developed and
 187 deployed at CREATIS laboratory. In 2021, VIP counts more than 1300
 188 registered users and approximately twenty applications. Taking advantage
 189 of computation resources made available by the EGI, VIP:

- 190 • makes scientific applications easily accessible as services within the plat-
 191 form,
- 192 • makes distributed computing resources easily accessible without tech-
 193 nical knowledge necessary on parallel computing,
- 194 • allows diffusion of applications at an international scale, for open and
 195 reproducible research.

196 VIP is present in multiple French projects and platforms at national scale
197 (France Grilles, France Life Imaging), and at international scale (EGI ACE,
198 EOSC). VIP is freely accessible for the worldwide research community.

199 MicroVIP deployment on VIP allows the user to run the software without
200 any installation procedure, dependencies or hardware constraints. Addition-
201 ally, VIP platform offers parallelization capabilities, allowing the generation
202 of a large number of simulated images by seamless execution on EGI, which
203 permits fast simulation of a large number of cell images and their associated
204 ground truth, needed for deep learning applications. An illustration of the
205 computation time (in hours) required for the simulation and textural fea-
206 tures extraction as a function of the number of cells simulated is presented
207 in figure 5. Simulation was performed for a light-sheet fluorescence micro-
208 scope with a microfluidic system. Figure 5.A displays total computation
209 time, which is the sum of execution times on each machine. This ignores file
210 transfer times between distributed sites, but gives an estimation of the com-
211 putation time that would be necessary for successively executing MicroVIP
212 complete pipeline a number of times equal to the number of cells to sim-
213 ulate. On the other hand, Figure 5.B displays real elapsed time between
214 the moment when the user launches and the output being accessible in their
215 VIP File Transfer. It takes into account file transfer times, but allows an
216 estimation of the time gained by running MicroVIP in a parallelized fashion
217 on EGI. For eleven executions with 1000 cells, we observe a median total
218 computation time of 148.0h, and a median real elapsed time of 4.1h, which
219 corresponds to an estimated parallelization time gain of more than 35 fold.
220 Variability for measured times is however important, as between two execu-
221 tions numerous factors can vary: EGI total load due to other users of the
222 service, network speed for file transfers, etc. More measures would there-
223 fore be needed in order to refine this estimation, but the order of magnitude
224 shows the added value provided by MicroVIP deployment on VIP for large
225 datasets simulation.

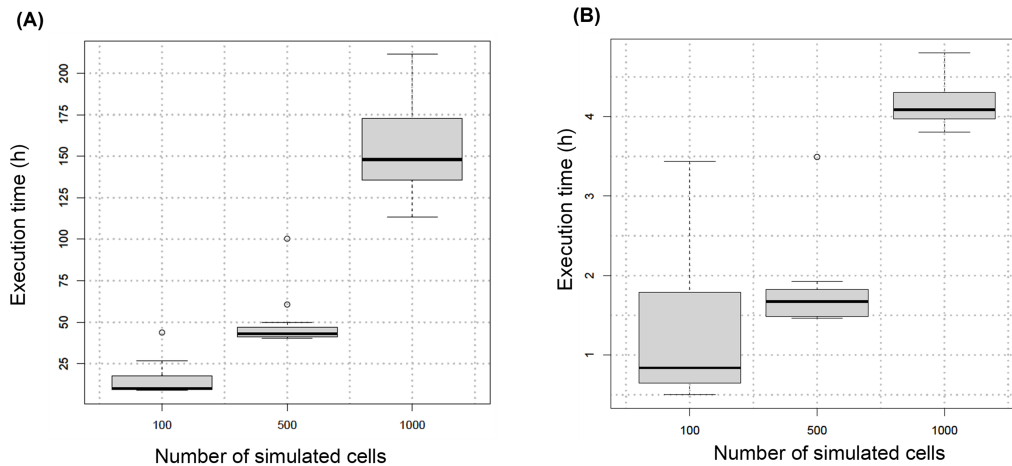


Figure 5: Median and standard deviation of simulation time with MicroVIP (in hours) as a function of the number of cells. For each number of cells, eleven executions were performed: (A) accumulated computation time of all parallel executions (B) real elapsed time between launch and end of MicroVIP execution, obtained by parallelizing computation on the EGI infrastructure.

226 5.2. Tutorial

227 MicroVIP was presented during International Symposium on Biomedical
 228 Imaging conference (IEEE ISBI 2021, April 13-16, 2021) tutorial session
 229 "A review of image annotation, augmentation and synthesis approaches for
 230 accelerating supervised machine learning in bioimaging". A hands-on was
 231 conducted, where participants simultaneously tested the application by simulating
 232 one cell under several imaging conditions. To this aim, six configuration
 233 files were prepared beforehand and made available under VIP
 234 File Transfer system, so that participants could simply select them to run
 235 simulations without needing to download and modify the configuration file
 236 themselves. Tested conditions were Widefield, Light-Sheet, Confocal, 2-
 237 beam and 3-beam Structured Illumination Microscopy without microfluidics,
 238 as well as Widefield with microfluidics (cell speeds of 140 and 400
 239 $\mu\text{m}/\text{s}$). A tutorial video for MicroVIP was recorded. It is available at
 240 <https://uabox.univ-angers.fr/index.php/s/rFQNUmlUkaXh2yQ>.

241 6. Conclusions

242 In this article, we presented MicroVIP, a microscopy image simulator that
 243 assembles the main fluorescence microscopies in a single web application. On

244 top of this generic functionality, MicroVIP also includes: (i) a specific use
245 case to generate single cells with markers located on chromatin (ii) a set of
246 standard textural textural and pointillist features to feed machine learning
247 algorithms.

248 We have illustrated the interest of this software to generate at high-
249 throughput large datasets for training machine learning algorithms or to
250 optimize optical systems via virtual instrumentation. The software is avail-
251 able for public use with an easy interface via Virtual Imaging Platform (VIP).
252 Its code is accessible online under GNU GPL license, along with a compre-
253 hensive documentation wiki.

254 MicroVIP already enabled realistic simulation of single-cell fluorescent
255 microscopy imaging for a wide variety of microscopes. Any further devel-
256 opment would still be possible, either by its authors or by the community
257 taking advantage of its open-source availability and its flexibility to host any
258 new application as a module executed from the command line, regardless of
259 its programming language.

260 **7. Conflict of Interest**

261 The authors declare that they have no known competing financial inter-
262 ests or personal relationships that could have appeared to influence the work
263 reported in this paper.

264 **Acknowledgements**

265 This work has been developed during the thesis of Ali AHMAD sup-
266 ported by project EU H2020 FET Open, PROCHIP, ” Chromatin orga-
267 nization PROfiling with high-throughput super-resolution microscopy on a
268 CHIP”, grant agreement no. 801336 (<https://pro-chip.eu/>). The appli-
269 cation presented in this work is available through the Virtual Imaging Plat-
270 form [29], using the resources provided by the biomed virtual organisation
271 of the EGI infrastructure. [https://operations-portal.egi.eu/vo/view/](https://operations-portal.egi.eu/vo/view/voname/biomed)
272 [voname/biomed](https://operations-portal.egi.eu/vo/view/voname/biomed)

273 **References**

- 274 [1] A. Lehmussola, P. Ruusuvuori, J. Selinummi, H. Huttunen, O. Yli-
275 Harja, Computational framework for simulating fluorescence microscope
276 images with cell populations, IEEE Transactions on Medical Imaging
277 26 (7) (2007) 1010–1016.

- 278 [2] H. Kirshner, F. Aguet, D. Sage, M. Unser, 3-d psf fitting for fluores-
279 cence microscopy: implementation and localization application, *Journal*
280 *of Microscopy* 249 (1) (2013) 13–25.
- 281 [3] H. Kirshner, D. Sage, M. Unser, 3d psf models for fluorescence mi-
282 croscopy in imagej, in: *Proceedings of the Twelfth International Confer-*
283 *ence on Methods and Applications of Fluorescence Spectroscopy, Imag-*
284 *ing and Probes (MAF'11)*, Vol. 154, 2011.
- 285 [4] S. Dmitrieff, F. Nédélec, Confocalgn: A minimalistic confocal image
286 generator, *SoftwareX* 6 (2017) 243–247.
- 287 [5] M. J. Nasse, J. C. Woehl, Realistic modeling of the illumination point
288 spread function in confocal scanning optical microscopy, *JOSA a* 27 (2)
289 (2010) 295–302.
- 290 [6] D. Wiesner, D. Svoboda, M. Maška, M. Kozubek, Cytovacq: a web-
291 interface for simulating multi-dimensional cell imaging, *Bioinformatics*
292 35 (21) (2019) 4531–4533.
- 293 [7] A. Girsault, T. Lukes, A. Sharipov, S. Geissbuehler, M. Leutenegger,
294 W. Vandenberg, P. Dedecker, J. Hofkens, T. Lasser, Sofi simulation tool:
295 a software package for simulating and testing super-resolution optical
296 fluctuation imaging, *PLoS One* 11 (9) (2016) e0161602.
- 297 [8] V. Venkataramani, F. Herrmannsdörfer, M. Heilemann, T. Kuner,
298 Suresim: simulating localization microscopy experiments from ground
299 truth models, *Nature Methods* 13 (4) (2016) 319–321.
- 300 [9] M. Lagardère, I. Chamma, E. Bouilhol, M. Nikolski, O. Thoumine, Flu-
301 osim: simulator of single molecule dynamics for fluorescence live-cell
302 and super-resolution imaging of membrane proteins, *Scientific Reports*
303 10 (1) (2020) 1–14.
- 304 [10] M. Weigert, K. Subramanian, S. T. Bundschuh, E. W. Myers,
305 M. Kreysing, Biobeam—multiplexed wave-optical simulations of light-
306 sheet microscopy, *PLoS Computational Biology* 14 (4) (2018) e1006079.
- 307 [11] S. Wang, J. Xu, J. Zeng, Inferential modeling of 3d chromatin structure,
308 *Nucleic Acids Research* 43 (8) (2015) e54–e54.
- 309 [12] A. Nwaneshiudu, C. Kuschal, F. H. Sakamoto, R. R. Anderson,
310 K. Schwarzenberger, R. C. Young, Introduction to confocal microscopy,
311 *Journal of Investigative Dermatology* 132 (12) (2012) 1–5.

- 312 [13] M. Saxena, G. Eluru, S. S. Gorthi, Structured illumination microscopy,
313 *Advances in Optics and Photonics* 7 (2) (2015) 241–275.
- 314 [14] J. Huisken, J. Swoger, F. Del Bene, J. Wittbrodt, E. H. Stelzer, Opti-
315 cal sectioning deep inside live embryos by selective plane illumination
316 microscopy, *Science* 305 (5686) (2004) 1007–1009.
- 317 [15] E. H. Stelzer, Light-sheet fluorescence microscopy for quantitative biol-
318 ogy, *Nature Methods* 12 (1) (2015) 23 – 26.
- 319 [16] C. Cremer, A. Szczurek, F. Schock, A. Gourram, U. Birk, Super-
320 resolution microscopy approaches to nuclear nanostructure imaging,
321 *Methods* 123 (2017) 11–32.
- 322 [17] M. A. Boland, E. A. Cohen, S. R. Flaxman, M. A. Neil, Improving axial
323 resolution in structured illumination microscopy using deep learning,
324 *Philosophical Transactions of the Royal Society A* 379 (2199) (2021)
325 20200298.
- 326 [18] H. Gong, W. Guo, M. A. Neil, Gpu-accelerated real-time reconstruction
327 in python of three-dimensional datasets from structured illumination
328 microscopy with hexagonal patterns, *Philosophical Transactions of the*
329 *Royal Society A* 379 (2199) (2021) 20200162.
- 330 [19] A. Ahmad, C. Frindel, D. Rousseau, Detecting differences of fluorescent
331 markers distribution in single cell microscopy: textural or pointillist
332 feature space?, *Frontiers in Robotics and AI* 7 (2020) 39.
- 333 [20] A. Ahmad, C. Frindel, D. Rousseau, Sorting cells from fluorescent mark-
334 ers organization in confocal microscopy: 3d versus 2d images, in: 2020
335 Tenth International Conference on Image Processing Theory, Tools and
336 Applications (IPTA), IEEE, 2020, pp. 1–6.
- 337 [21] T. Ojala, M. Pietikäinen, T. Mäenpää, Multiresolution gray-scale and
338 rotation invariant texture classification with local binary patterns, *IEEE*
339 *Transactions on Pattern Analysis & Machine Intelligence* 24 (7) (2002)
340 971 – 987.
- 341 [22] G. Zhao, M. Pietikainen, Dynamic texture recognition using local binary
342 patterns with an application to facial expressions, *IEEE Transactions on*
343 *Pattern Analysis & Machine Intelligence* 29 (6) (2007) 915–928.
- 344 [23] R. M. Haralick, K. Shanmugam, et al., Textural features for image clas-
345 sification, *IEEE Transactions on Systems, Man, and Cybernetics* 3 (6)
346 (1973) 610 – 621.

- 347 [24] E. B. Othmen, M. Sayadi, F. Fnaiech, 3 d gray level co-occurrence matrices for volumetric texture classification, in: 3rd International Conference on Systems and Control, IEEE, 2013, pp. 833–837.
348
349
- 350 [25] J. Bruna, S. Mallat, Invariant scattering convolution networks, IEEE Transactions on Pattern Analysis and Machine Intelligence 35 (8) (2013) 1872–1886.
351
352
- 353 [26] B. D. Ripley, Statistical inference for spatial processes, Cambridge university press, 1991.
354
- 355 [27] S. Mailfert, J. Touvier, L. Benyoussef, R. Fabre, A. Rabaoui, M.-C. Blache, Y. Hamon, S. Brustlein, S. Monneret, D. Marguet, et al., A theoretical high-density nanoscopy study leads to the design of unloc, a parameter-free algorithm, Biophysical Journal 115 (3) (2018) 565–576.
356
357
358
- 359 [28] M. Weigert, U. Schmidt, T. Boothe, A. Müller, A. Dibrov, A. Jain, B. Wilhelm, D. Schmidt, C. Broaddus, S. Culley, et al., Content-aware image restoration: pushing the limits of fluorescence microscopy, Nature Methods 15 (12) (2018) 1090–1097.
360
361
362
- 363 [29] T. Glatard, C. Lartizien, B. Gibaud, R. F. Da Silva, G. Forestier, F. Cervenansky, M. Alessandrini, H. Benoit-Cattin, O. Bernard, S. Camarasu-Pop, et al., A virtual imaging platform for multi-modality medical image simulation, IEEE Transactions on Medical Imaging 32 (1) (2012) 110–118.
364
365
366
367

368 Appendix A. Example .ini configuration file

```
369 ; Default parameter file for MicroVIP applicatons.
370 ; See https://www.creatis.insa-lyon.fr/site7/en/PROCHIP for more information.
371
372 ; This parameter file is divided in three sections, each one used
373 ; by one module of MicroVIP application. If you do not run all three
374 ; modules, you may leave unrelevant sections unmodified. They will
375 ; be ignored at runtime. You can modify other parameters at will after
376 ; carefully reading their description.
377
378 ;-----
379 ; Module 1: Generation of biological objects
380 ;-----
381 ; This section contains modeled ground truth biological parameters.
382 ; These are random distributions from which the cell size and the distances
383 ; between consecutive biomarkers are drawn, as well as the number of chromatin
384 ; chains inside each cell.
385 [CellGenerator]
386 ; Number of chromatin chains (chromosomes) in one cell.
387 n_chromatin_chain=46
388 ; Fluorophore will be generated along chomatin chains with random distances
389 ; picked from following distribution: u for uniform or g for gaussian.
390 marker_distribution_type=u
391 ; If uniform distribution: lower bound of the interval.
392 ; If Gaussian distribution: mean value
393 ; (arbitrary unit)
394 marker_distribution_param1=0
395 ; If uniform distribution: upper bound of the interval.
396 ; If Gaussian distribution: standard deviation
397 ; (arbitrary unit)
398 marker_distribution_param2=50
399 ; Cell size in each axis will be picked from given distribution:
400 ; u for uniform or g for gaussian.
401 cell_size_distribution_type=u
402 ; If uniform distribution: lower bound of the interval.
403 ; If Gaussian distribution: mean value
404 ; ( $\mu\text{m}$ )
405 cell_size_distribution_param1=5
406 ; If uniform distribution: upper bound of the interval.
407 ; If Gaussian distribution: standard deviation
408 ; ( $\mu\text{m}$ )
409 cell_size_distribution_param2=12
```

```

410
411 ;-----
412 ; Module 2: Microscopy image Simulation
413 ;-----
414 ; This section defines the type of microscope to simulate and its optical
415 ; parameters, as well as image acquisition system configuration (camera size,
416 ; shutter speed...). As MicroVIP allows simulation of moving objects as found
417 ; in microfluidic systems, this section also defines imaged cell speed.
418 ; Super-resolution acquisition methods are simulated using third-party code
419 ; SOFIsim~\cite{girsault2016sofi} which requires additional parameters found
420 ; in this section, such as acquisition duration, CCD structure conversion and
421 ; noise constants.
422 [MicroscopySimulator]
423 ; Microscope type: 0, 1, 2, 3, 4, or 5, respectively for widefield, confocal,
424 ; 2 beam Structured Illumination Microscopy (SIM), 3 beam SIM, STORM and
425 ; balanced SOFI (bSOFI).
426 ; Notes:
427 ; Only widefield, 2-beam and 3-beam SIM can be used with microfluidics
428 ; (cell_speed > 0)
429 ; Only widefield, confocal, 2-beam and 3-beam SIM can be used with light-sheet
430 ; (fwhmz > 0)
431 microscope=0
432 ; Emission wavelength ( $\mu\text{m}$ ).
433 wavelength=0.5
434 ; Refractive index at sample (water immersion n=1.33, dry n=1, oil n =1.51).
435 refractive_index=1.33
436 ; Numerical aperture of the optical system.
437 numerical_aperture=1.25
438 ; Camera pixel size ( $\mu\text{m}$ ).
439 pixel_size_um=6.5
440 ; Objective magnification.
441 magnification=60
442 ; Camera width and length (pixels). For Widefield, confocal, 2-beam and 3-beam
443 ; SIM, it corresponds to final microscopy image lateral size. For STORM and
444 ; bSOFI, supe-resolution algorithm produces a larger final image.
445 camera_size_px=256
446 ; Imaged area extends from -axial_range_um to +axial_range_um in axial
447 ; dimension ( $\mu\text{m}$ ).
448 axial_range_um=5
449 ; Step size in axial direction ( $\mu\text{m}$ ). Final image is a stack of 2D images from
450 ; "slices" in the imaged object, distant from one another by axial_step_um  $\mu\text{m}$ .
451 ; This value is ignored if microfluidics is used (cell_speed > 0), as it is then
452 ; determined from cell speed and camera frame rate.

```

```

453 axial_step_um=0.3
454 ; Camera shutter speed, inverse of exposure time (s-1)
455 shutter_speed_hz=200
456 ; Camera frame rate (frame/s). Usually half of shutter speed value.
457 frame_rate_hz=100
458 ; Expected number of photons emitted by a single fluorophore. This is a
459 ; parameter of Poisson noise simulation.
460 marker_intensity_photon=100
461 ; Mean of additive Gaussian noise. By default Gaussian noise intensity should be
462 ; adjusted by changing gaussian_noise_std and letting gaussian_noise_mean be 0.
463 gaussian_noise_mean=0
464 ; Standard deviation of additive Gaussian noise.
465 gaussian_noise_std=0.5
466 ; Average bleaching time of the biomarkers (s). 0 deactivates photobleaching
467 ; simulation.
468 bleaching_time_s=0.5
469 ; Cell speed inside microfluidic system (µm/s), used for motion blur simulation.
470 ; 0 deactivates motion blur (corresponding to a standard system without
471 ; microfluidics). Note that confocal, STORM and bSOFI microscopes do not support
472 ; microfluidic system, so please ensure cell_speed_um_per_s=0 for these
473 ; microscopy techniques.
474 cell_speed_um_per_s=20
475 ; Full Width at Half Maximum (FWHM) of Gaussian Point Spread Function (PSF) in
476 ; axial direction, ie width of a light sheet (µm). 0 deactivates light-sheet
477 ; microscopy. Note that STORM and bSOFI simulation do not support light-sheet
478 ; microscopy, so light_sheet_width_um is ignored for these microscopy
479 ; techniques.
480 light_sheet_width_um=2.9
481
482 ;; This parameter is used only for 3-beam SIM. For other microscopes, simply
483 ;; leave it as is
484 ; Wiener filter parameter for 3-beam SIM final image reconstruction
485 wiener_parameter=0.1
486
487 ;; Following parameters are only used for STORM and balanced SOFI simulations.
488 ; Radius of a biomarker (nm).
489 marker_radius_nm=8
490 ; Average time (ms) during which a biomarker is active, i.e. emitting photons.
491 marker_on_lifetime_ms=20
492 ; Average time (ms) during which a biomarker is inactive, i.e. dark.
493 marker_off_lifetime_ms=40
494 ; Time over which the camera records the fluorescence signal (s).
495 acquisition_duration_s=3

```

```

496 ; Mean number of electrons generated in the CCD structure for one incoming
497 ; photon (electrons/photon).
498 quantum_gain=4.2
499 ; Intensity of fluorescence not emitted from the biomarkers (photons). In a cell
500 ; sample, this background could arise from auto-fluorescence, i.e. fluorescence
501 ; emission from small biological molecules such as NADH.
502 background_intensity_photon=0
503 ; Intensity of a second additive readout noise, arising from the stochastic
504 ; thermal generation of electrons within the CCD structure (electrons/pixel/s).
505 dark_current=0
506
507 ;-----
508 ; Module 3: Features extraction
509 ;-----
510 ; This section contains hyper-parameters of all applied features extraction
511 ; methods. It also provides an option to de-activate pointillist features
512 ; extraction methods which are particularly time-consuming as they require an
513 ; additional step of biomarkers localization.
514 [FeaturesExtractor]
515 ;; Following parameters are used for 2D features extraction.
516 ;; This extraction is performed over the image's sum z-projection.
517 ; Distance (pixels) between paired pixels for 2D Gray Level Co-occurrence Matrix
518 ; (GLCM) calculation, used in Haralick features extraction.
519 neighborhood_size_GLCM_2D=8
520 ; Number of neighbors used to compute the Local Binary Pattern (LBP) for each
521 ; pixel. The set of neighbors is selected from a circularly symmetric pattern
522 ; around each pixel. Higher values encode greater detail around each pixel.
523 ; Typical values range from 4 to 24.
524 n_neighbor_LBP_2D=8
525 ; Radius (pixels) of circular pattern used to select neighbors for each pixel in
526 ; LBP calculation. Higher values capture detail over a larger spatial scale.
527 ; Typical values range from 1 to 5.
528 radius_LBP_2D=1
529 ; Maximal order of the scattering transform, i.e. depth of associated scattering
530 ; network. When set to 1, the scattering transform is merely the modulus of a
531 ; wavelet transform. In most cases, higher values marginally improve
532 ; classification results, yet at a great computational cost.
533 n_layer_scattering_2D=2
534 ; Number of wavelet scales in the filter bank for scattering transform
535 ; computation. Higher values increase the range of translation invariance.
536 n_scale_scattering_2D=4
537 ; Number of wavelet orientations for scattering transform computation. Higher
538 ; values increase the angular selectivity of filters.

```

```

539 n_orientation_scattering_2D=8
540
541 ;; Following parameters are used for 3D features extractions.
542 ;; This extraction is performed directly over the 3D microscopy image.
543 ; Distance (pixels) between paired pixels for 3D GLCM calculation, used in
544 ; 3D Haralick features extraction.
545 neighborhood_size_GLCM_3D=8
546 ; Number of pixel neighbors respectively in XY, XZ and YZ plane of the image for
547 ; LBP-TOP computation. The set of neighbors is selected from a circularly
548 ; symmetric pattern around each pixel. Higher values encode greater detail
549 ; around each pixel. Accepted values are 4, 8, 16 and 24, with 8 being
550 ; recommended.
551 n_xy_neighbor_LBPTOP=8
552 n_xz_neighbor_LBPTOP=8
553 n_yz_neighbor_LBPTOP=8
554 ; Radius (pixels) of circular pattern used in LBP-TOP computation to select
555 ; neighbors for each pixel, respectively along first, second and third dimension
556 ; of the image. Accepted values are 1, 2, 3 and 4, and recommended values are 1
557 ; and 3. Note that radius * 2 + 1 should be smaller than image size in
558 ; corresponding dimension. For example, for an image stack of seven images
559 ; (i.e. size in Z is 7), z_radius_LBPTOP=3 means only the pixels in frame 4 can
560 ; be considered as central pixel and have LBP-TOP features computed.
561 x_radius_LBPTOP=1
562 y_radius_LBPTOP=1
563 z_radius_LBPTOP=3
564 ; Same as n_layer_scattering_2D, n_scale_scattering_2D and
565 ; n_orientation_scattering_2D for 3D scattering transform (i.e. scattering
566 ; transform of x, y and z sum projections).
567 n_layer_scattering_3D=2
568 n_scale_scattering_3D=4
569 n_orientation_scattering_3D=8
570 ; Should pointillist features be extracted (0 for no, 1 for yes)?
571 extract_pointillist=1
572
573 ;; Following parameters are ignored if extract_pointillist=0.
574 ; Radius step size (µm) for Ripley K-function discretized estimation.
575 radius_step_ripley_um=0.2
576 ; Maximum radius (µm) for Ripley K-function estimation.
577 max_radius_ripley_um=13
578 ; Minimum and maximum number of markers in a cluster for Voronoi features
579 ; extraction.
580 min_cluster_size_Voronoi=5
581 max_cluster_size_Voronoi=50

```